Electronic Supplementary Material (ESI) for Journal of Materials Chemistry A.

Supporting Information

Dense Organic Molecules/graphene Network Anodes with Superior Volumetric and Areal Performance for Asymmetric Supercapacitors

Lina Zhang,‡[ab] Daliang Han,‡[ab] Ying Tao,[ab] Changjun Cui,[ab] Yaqian Deng,[c] Ximan Dong,[ab] Wei Lv,[c] Zifeng Lin,[d] Shichao Wu,[ab] Zhe Weng,*[ab] and Quan-Hong Yang*[ab]

[a] Nanoyang Group, State Key Laboratory of Chemical Engineering School of Chemical Engineering and Technology, Tianjin University, Tianjin 300350, China, E-mail: zweng@tju.edu.cn; qhyangcn@tju.edu.cn

[b] Joint School of National Singapore and Tianjin University, International Campus of Tianjin University, Binhai New City, Fuzhaou 350207, China.

[c] Shenzhen Key Laboratory for Graphene-based Materials, Graduate School at Shenzhen, Tsinghua University, Shenzhen 518055, China.

[d] College of Materials Science and Engineering, Sichuan University, Chengdu 610065, China.

‡ These two authors are equal major contributors to this work.

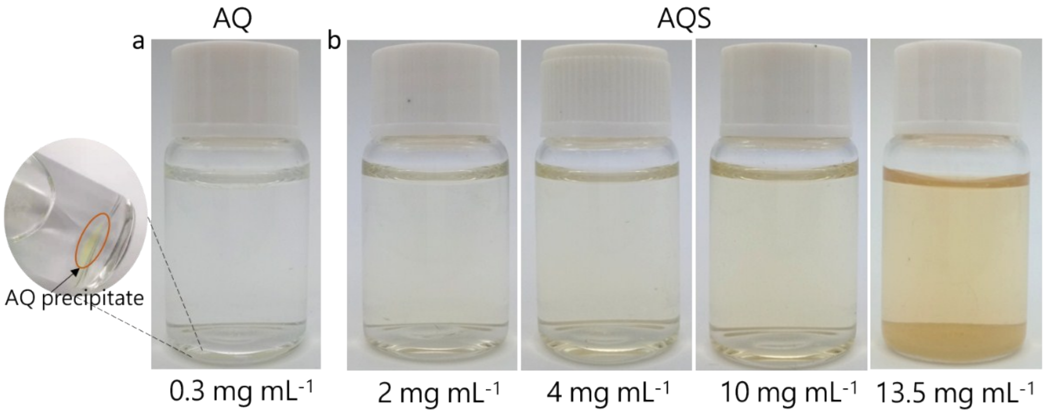

Fig. S1 (a) Solubility of anthraquinone (AQ) and (b) anthraquinone-2-sulfonate (AQS) with different concentration.

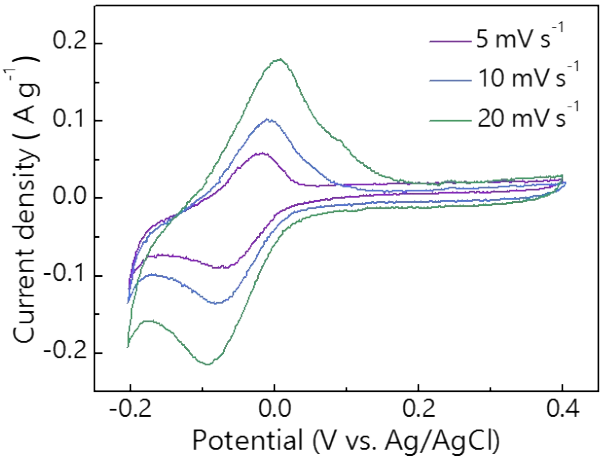

Fig. S2 Cyclic voltammetry profiles of pure AQS.

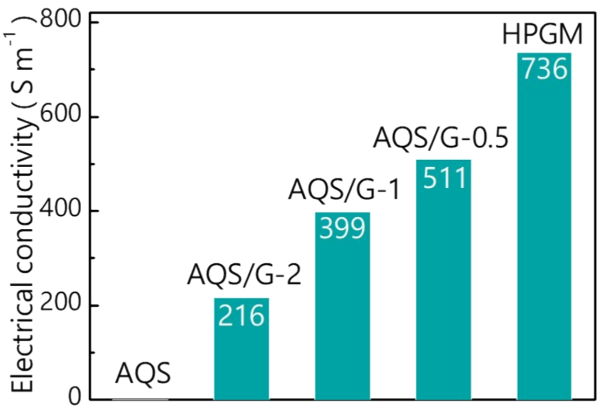

Fig. S3 Electrical conductivity of pure AQS, HPGM and AQS/Gs with various AQS loading.

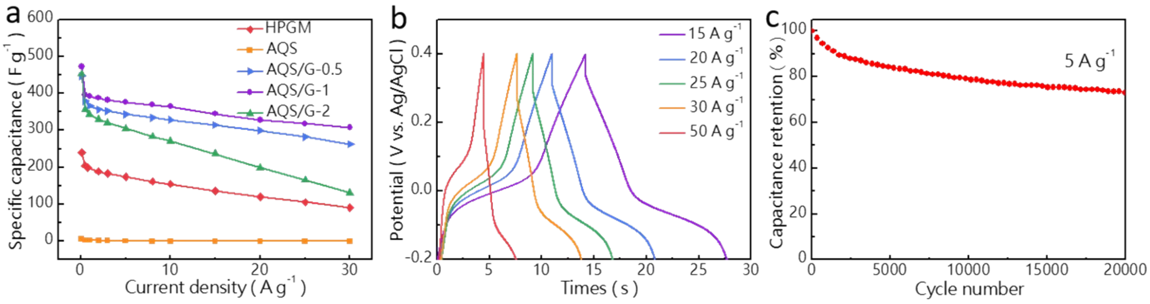

Fig. S4 (a) Gravimetric specific capacitances of HPGM, AQS and AQS/Gs with different AQS mass loading. (b) Galvanostatic charge-discharge curves of AQS/G-1 at high current densities. (c) Cycling performance of AQS/G-1.

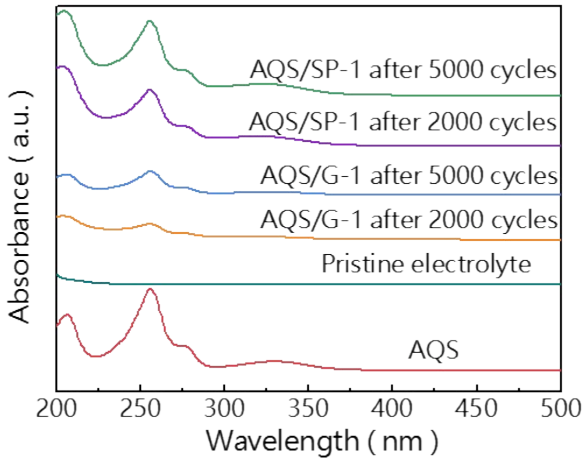

Fig. S5 UV-vis spectra of pure AQS aqueous solution, and the electrolyte before and after cycling.

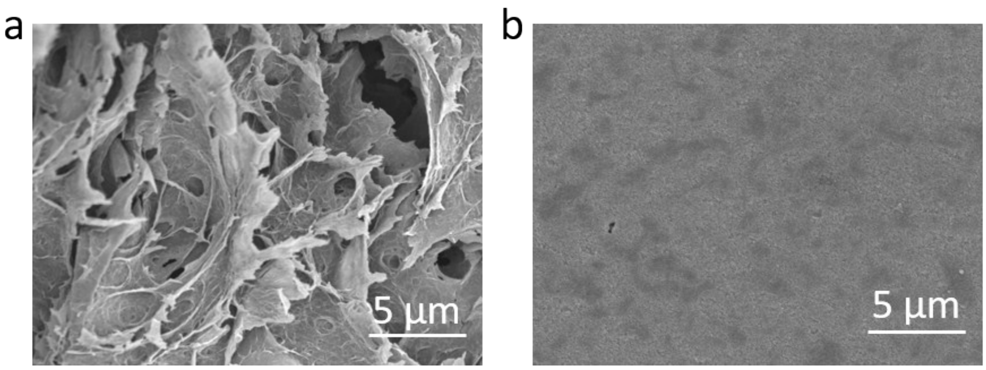

Fig. S6 SEM image of (a) AQS/G-1 xerogel and (b) compact AQS/G-1.

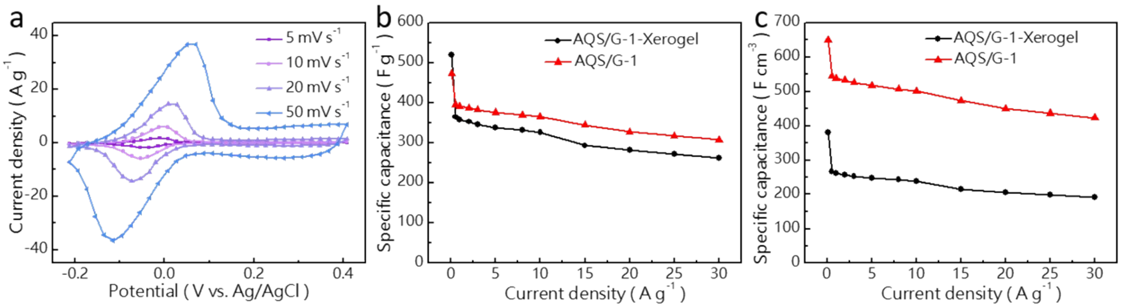

Fig. S7 (a) CV curves, (b) gravimetric and (c) volumetric specific capacitances of AQS/G-1 xerogel after freezing drying.

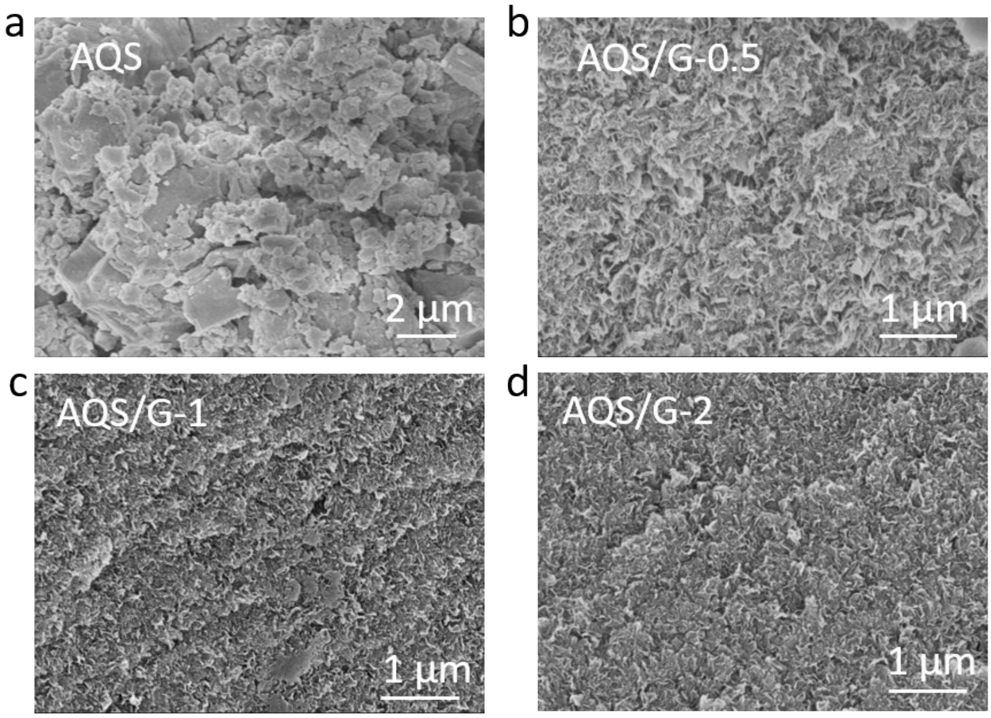

Fig. S8 SEM images of (a) AQS, (b) AQS/G-0.5, (c) AQS/G-1 and (d) AQS/G-2.

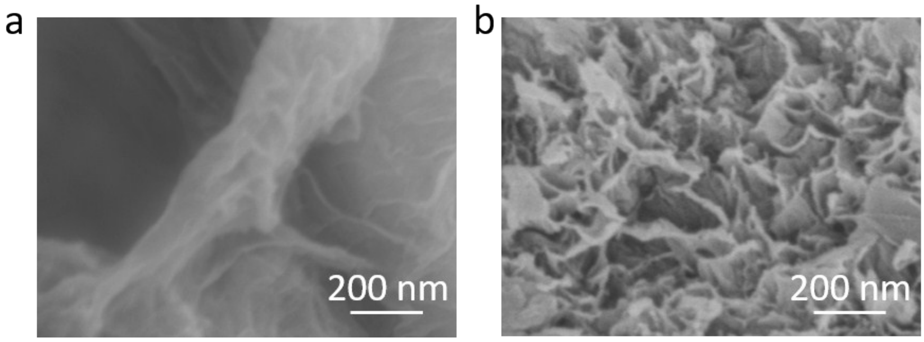

Fig. S9 High magnification SEM images of (a) AQS/G-1 xerogel and (b) compact AQS/G-1.

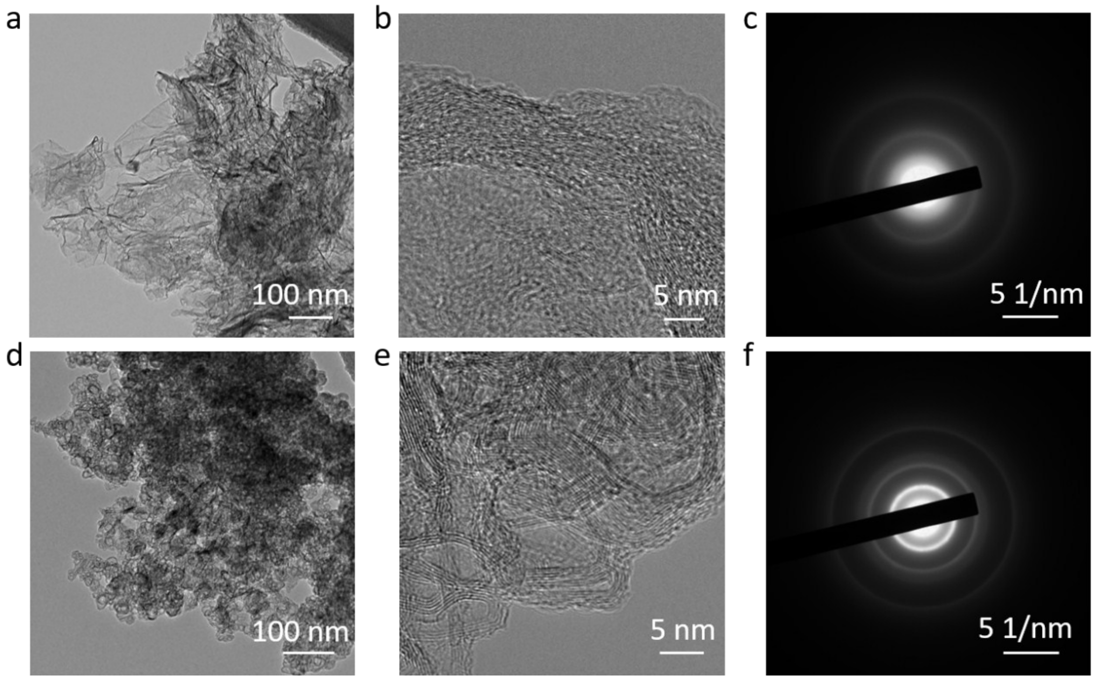

Fig. S10 (a) TEM image and (b) HRTEM image of AQS/G-1. (c) Corresponding selected area electron diffraction (SEAD) image of AQS/G-1. (d) TEM image and (e) HRTEM image of AQS. (f) Corresponding SEAD image of AQS.

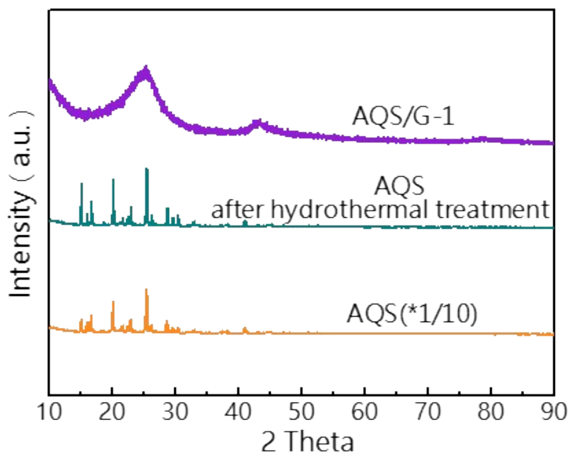

Fig. S11 XRD patterns of pristine AQS, AQS/G-1 and pure AQS after hydrothermal treatment.

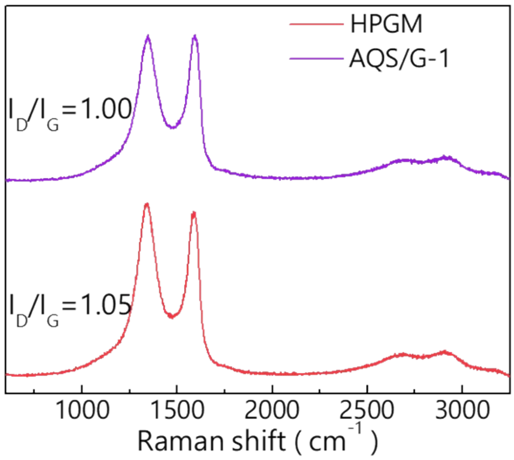

Fig. S12 Raman spectra of HPGM and AQS/G-1.

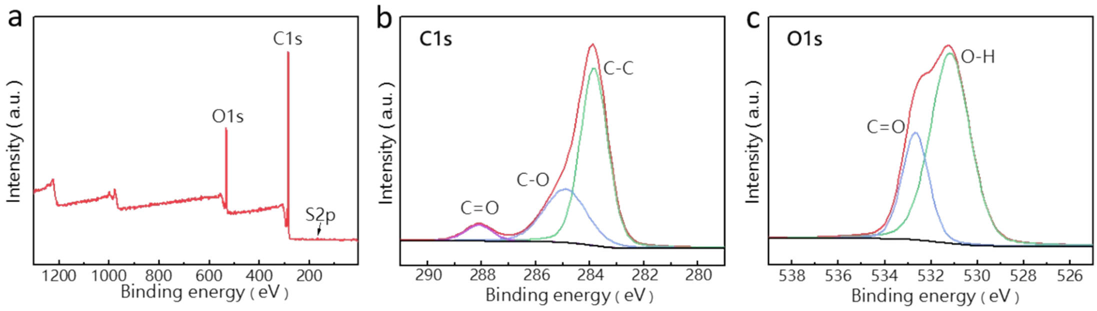

Fig. S13 (a) Survey XPS spectrum of AQS/G-1. (b) XPS high-resolution spectra of C1s and (c) O1s.

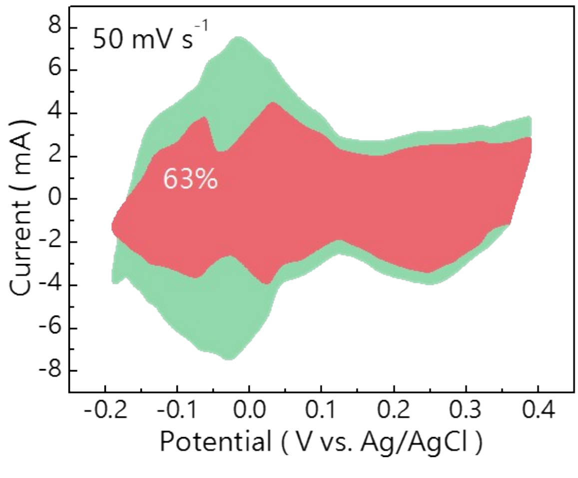

Fig. S14 Capacitive contribution to the total charge at a scan rate of 50 mV s^{-1}.

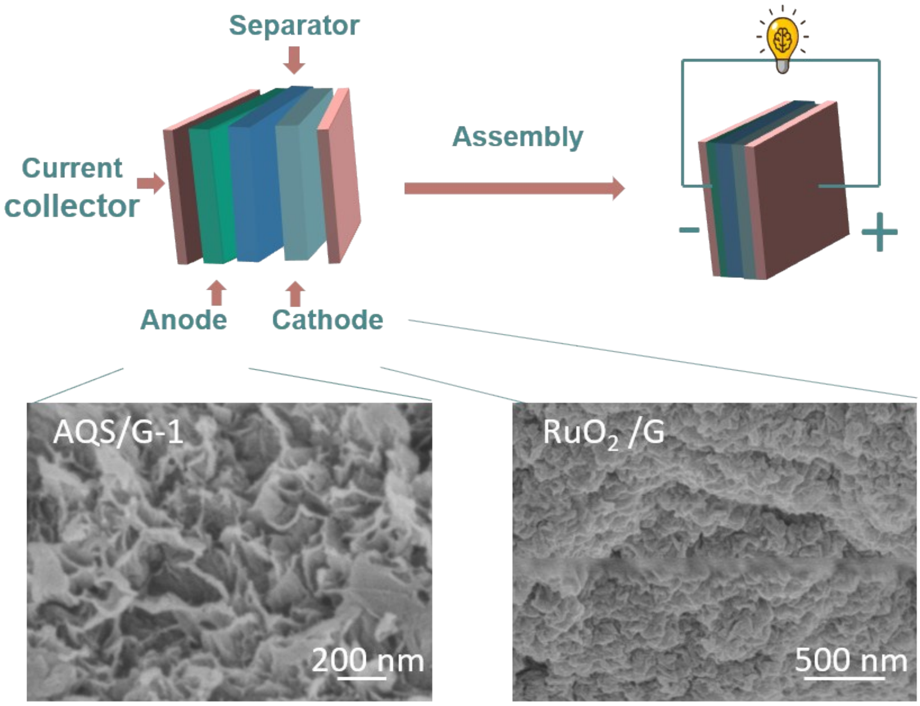

Fig. S15 Schematical illustration of the asymmetric supercapacitor fabrication process with AQS/G-1 as the anode and RuO_2/G as the cathode.

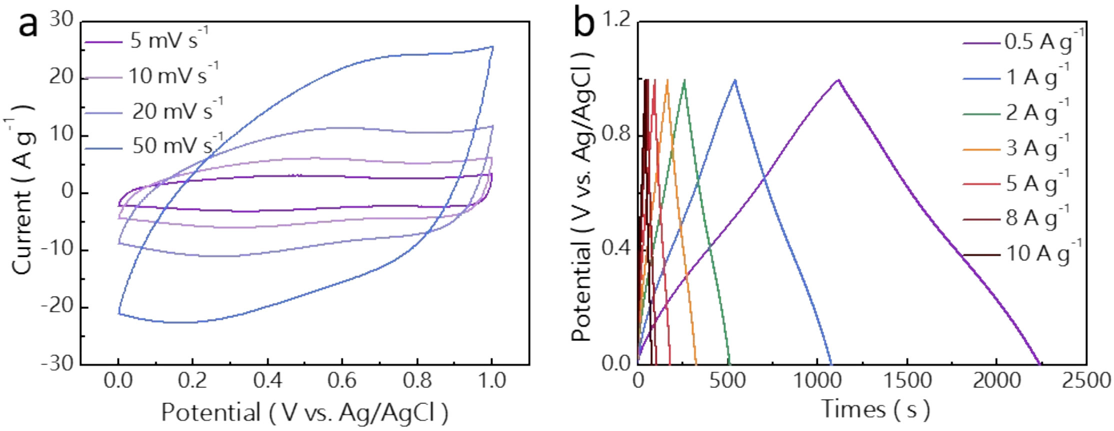

Fig. S16 (a) Cyclic voltammetry profiles and (b) galvanostatic charge-discharge curves of RuO_2/G.

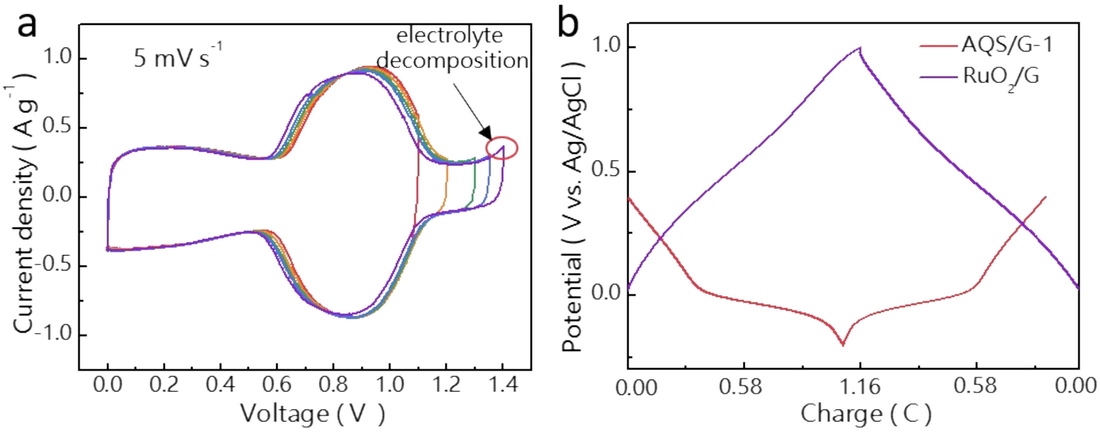

Fig. S17 (a) Cyclic voltammetry profiles of the AQS/G-1//RuO_2/G ASC at different operating voltages at a constant scan rate of 5 mV s^{-1}. (b) Galvanostatic charge-discharge curves of AQS/G-1 and RuO_2/G in different potential windows at a current density of 0.5 A g^{-1}.

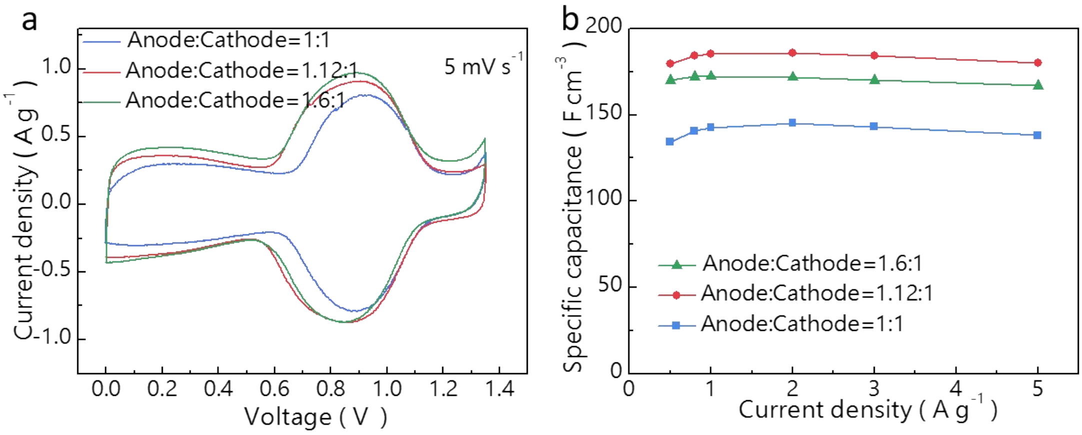

Fig. S18 (a) CV curves and (b) volumetric sepcific capacitance of the ASCs with various mass ratios (AQS/G-1 to RuO_2/G).

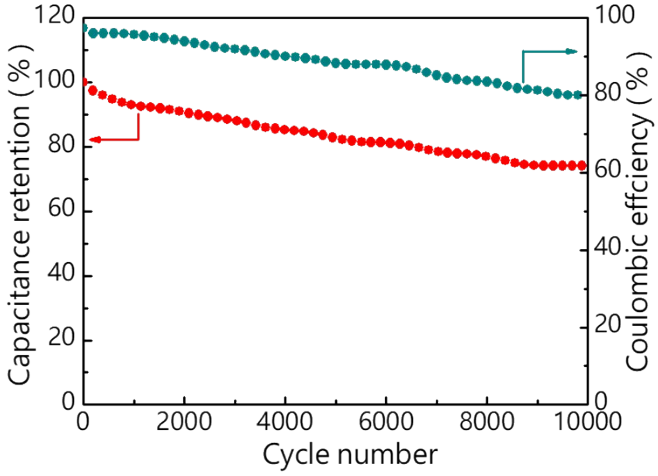

Fig. S19 Cycling performance of the AQS/G-1//RuO_2/G asymmetric supercapacitor.